analytical chemistry

Caltech Library

Subscriber access provided by Caltech Library

Article

In Situ Quantification of Surface Intermediates and Correlation to Discharge Products on Hematite Photoanodes using a Combined Scanning Electrochemical Microscopy Approach

Mihail R Krumov, Burton H. Simpson, Michael J Counihan, and Joaquin Rodriguez-Lopez

Anal. Chem., **Just Accepted Manuscript** • DOI: 10.1021/acs.analchem.7b04896 • Publication Date (Web): 02 Feb 2018

ACS Publications

Analytical Chemistry is published by the American Chemical Society. 1155 Sixteenth Street N.W., Washington, DC 20036

In Situ Quantification of Surface Intermediates and Correlation to Discharge Products on Hematite Photoanodes using a Combined Scanning Electrochemical Microscopy Approach

Mihail R. Krumov, [&,‡] Burton H Simpson, [&,‡,†] Michael J. Counihan[&], Joaquín Rodríguez-López[&,#,*]

[&] Department of Chemistry, University of Illinois at Urbana-Champaign, 600 South Mathews Avenue, Urbana, IL 61801*Corresponding author e-mail: joaquinr@illinois.edu; Phone: +1 (217) 300-7354.

[#] Beckman Institute for Advanced Science and Technology, University of Illinois at Urbana-Champaign

ABSTRACT: Hematite is a promising photoanode for solar driven water splitting. Elucidating its surface chemical pathways is key to improving its performance. Here, we use redox titrations in the Surface Interrogation mode of Scanning Electrochemical Microscopy (SI-SECM) to quantitatively probe *in situ* the reactivity and time evolution of surface species formed on hematite during photo assisted water oxidation. Using SI-SECM, two distinct populations of oxidizing surface species were resolved with measured k_{si} of 316 $m^3/(mol{\cdot}s)$ and 2 $m^3/(mol{\cdot}s)$ for the more and less reactive species respectively. While the surface coverage of both species was found to increase as a function of applied bias, the rate constants did not change appreciably, suggesting that the mechanism of water oxidation is independent of bias potential. In the absence of applied potential, both populations exhibit decay that is well described by second order kinetics, with k_d values of $1.2\times10^5 \pm 0.2\times10^5$ and $6.3\times10^3 \pm 0.9\times10^3$ $m^2/(mol{\cdot}s)$ for the fast and slow reacting adsorbates, respectively. Using transient substrate generation/ tip collection mode, we detected the evolution of as much as 1.0 μmol/m^2 of H_2O_2 during this decay process, which correlates with the coverage observed by one of the titrated species. By deconvoluting the reactivity of multiple adsorbed reactants, these experiments demonstrate how SI-SECM enables direct observation of multiple adsorbates and reaction pathways on operating photoelectrodes.

Hematite is a promising photoanode for solar driven water splitting because of its narrow band gap, chemical stability and elemental abundance.[1,2] However, even the best performing hematite photocatalysts exhibit efficiencies far below the theoretical maximum.[3] Slow water oxidation kinetics that take seconds to complete a full catalytic cycle are a major factor contributing to its poor performance.[4] Photocatalytic water oxidation is a complex electron and proton transfer process that proceeds through reactive surface states (RSS) of hematite.[4] These surface states are often reactive oxygen species (ROS) that are direct intermediates of the water oxidation reaction, but these states can also be parasitic surface species that trap holes and serve as recombination centers.[4] Because RSSs are crucial to the water oxidation reaction, elucidating their nature is central to strategies aimed at enhancing hematite's photocatalytic performance.

The need to fill this knowledge gap has led to several recent works elucidating the surface species involved in water oxidation on hematite. Studies utilizing photoelectrochemical impedance spectroscopy[5-7] or derivatives such as intensity modulated photocurrent spectroscopy[8-10] have observed an accumulation of surface states during water oxidation on hematite that were proposed to be Fe (IV) and Fe(V) states in the form of M-OH_x species. Klahr, et. al. observed that the decay kinetics of the accumulated states were consistent with the formation of Fe(IV) species that react bimolecularly to generate O_2 and that a critical coverage of these species was necessary for the onset of O_2 evolution.[7] Transient absorption spectroscopy also shows evidence of long-lived trapped holes on the surface of hematite that appear to be intermediates of water oxidation.[11-13] It was only recently that Zandi, et. al. reported their use of operando infrared spectroscopy to positively identify Fe^{IV}=O one form of the long-lived holes.[14] This study also observed the presence of an additional photogenerated species hypothesized to be Fe^{IV}-O-Fe^{IV} or Fe^{IV}-O-O-Fe^{IV}, but were unable to unambiguously identify this species or rule out M-OH_x species. Despite identifying Fe^{IV}=O as a key intermediate of water oxidation on hematite, Zandi concluded that further investigation is needed to resolve both the identities and kinetics of other surface species involved in water oxidation on hematite.

Although the aforementioned studies established Fe^{IV}=O as a key intermediate of water oxidation on hema-

tite, a more thorough understanding of the interfacial reactivity of surface species can better elucidate the role each species plays in the overall reactive mechanism. Knowing whether these species cooperate to oxidize water or represent intermediates of mechanisms competing for active sites will inform attempts to produce better hematite photoelectrodes. The techniques employed previously to probe decay kinetics at hematite surfaces lacked selectivity for surface species, provided limited quantification of coverage, and did not offer a direct measurement of reactivity. Scanning electrochemical microscopy (SECM) is a versatile electrochemical platform used in the characterization of electrocatalysts and photoelectrodes to collect products[15,16] and measure electron transfer kinetics.[17,18] Recently, the surface interrogation mode of SECM (SI-SECM) was introduced to probe reactive intermediates at catalytic surfaces,[19] and our group and others have since demonstrated its use for detection of ROS on operating photoelectrode surfaces.[20-24] SI-SECM uses a redox mediator to redox titrate species on substrates of interest, and enables the quantification of the surface coverage,[25] reaction kinetics, and spatial distribution[24] of adsorbed chemical intermediates of (electro)catalytic reactions.

SI-SECM is performed in two steps, as shown in Figure 1A. In the first step, light and/or external bias are applied to the substrate to initiate catalysis and populate the surface with intermediates. After this, the driving force is removed and a small tip electrode positioned close to the surface is activated to electrochemically generate a titrant *in situ* from a mediator in solution. The titrant diffuses to the substrate and reacts with redox-active surface species. This regenerates the mediator, producing a transient positive feedback current, shown in Figure 1B, that decays as the surface species are consumed. A background signal, where no catalysis occurs, is recorded by repeating the experiment without illuminating the substrate. Background subtraction removes contributions from charging current, other solution processes, and any non PEC surface process from the tip current. Because it is selective to surface species, quantitative for both surface coverage and reactivity, and operates over the large range of spatial and temporal scales relevant to the kinetics of water oxidation,[23] SI-SECM is ideal for studying adsorbed reaction intermediates formed on hematite.

Here, we use the multimodal functionality of SECM to investigate the role of RSS in the chemistry of water oxidation on thin film samples of hematite. Two distinct populations of photogenerated RSS were identified by their drastically differing reaction kinetics with our titrant species. Both species show potential-dependent coverages that increase proportionally with photocurrent, suggesting that both are related to water oxidation activity on the hematite surface. Delayed titrations showed that both populations decayed over time following second order kinetics with rate constants differing by an order of magnitude. These results prompted transient collection experiments that detected small quantities of H_2O_2 generated during the decay of these species, which can be from disproportionation reactions between hydroxyl radicals on the surface. As *oxo* species are considered to be the primary intermediate in water oxidation on hematite, these results suggest how side reactions might contribute to the low efficiency of hematite photoanodes.

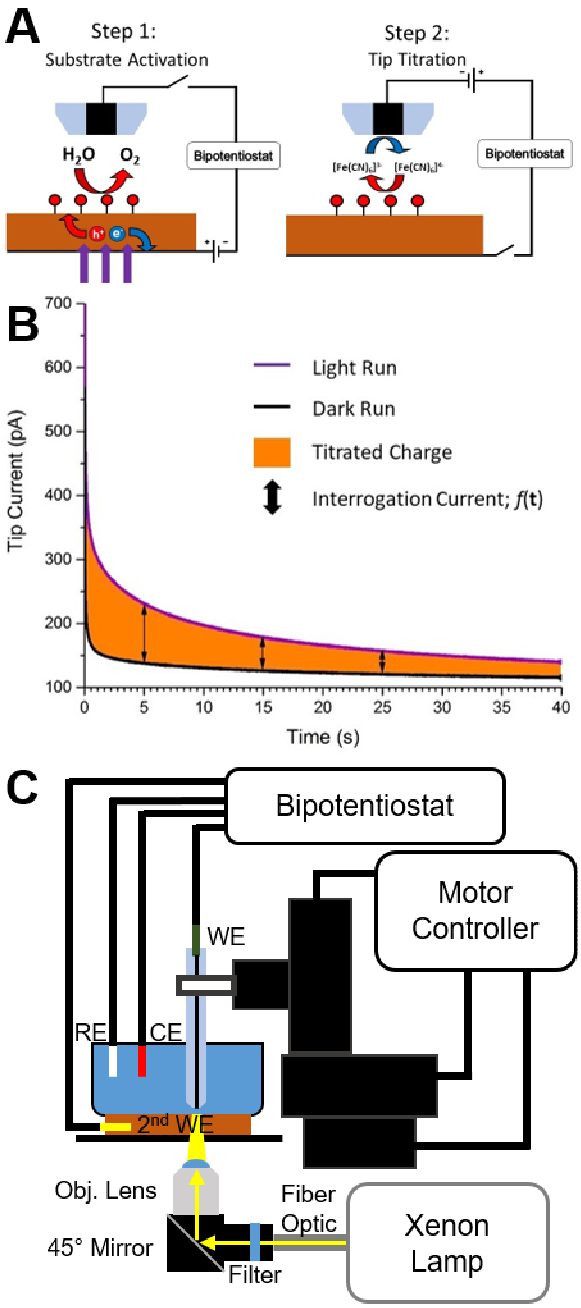

Figure 1: (A) Schematic of SI-SECM. In the first step, the substrate is activated through illumination and/or external bias to initiate catalysis, generating adsorbed intermediates. The probe remains inactive. In the second step, bias and illumination are removed so PEC processes cease at the substrate. The SECM probe is biased to activate an electrochemical mediator which diffuses to the surface and titrates the adsorbate in situ. (B) Titration of adsorbate generates a transient feedback loop of mediator which is recorded by the tip as a current signal. A dark run is performed for background subtraction to produce the interrogation current. (C) Block diagram of the SECM and illumination setup.

EXPERIMENTAL SECTION

Chemicals

Fluorine doped tin oxide (FTO) coated glass slides (R_s<= 14 Ω) were purchased from Delta Technologies, Limited. Acetone (99.5%, Sigma-Aldrich), chromatography grade water (Macron, ChromAR), and ethanol (Anhydrous, Decon Labs, Inc.) were used without further purification. Ferric chloride (anhydrous 98% Aldrich Chemical Company), titanium butoxide (Sigma-Aldrich), and hydrochloric acid (37.2% Fisher Scientific), potassium ferricyanide (99% Fisher Scientific), boric acid (99.5% Fisher Scientific), and sodium hydroxide (97% Fisher Scientific) were used as received. Gold and platinum wires for SECM tip fabrication were purchased from Goodfellow (Coraopolis, PA), while carbon fibers were purchased for Alfa Aesar.

Preparation of hematite electrodes

Hematite photoanodes were fabricated using methods adapted from Wang et. al.[26] Briefly, FTO coated slides were cleaned by sonication for 10 minutes each in acetone, chromatography grade water, and ethanol. Then, an ethanol solution of 10 mM $FeCl_3$, 1 mM titanium butoxide, and 40 mM HCl was prepared and drop deposited onto the FTO substrate. After 30 seconds, excess solution was blown off the FTO surface with compressed air, and the substrate was placed on a hot plate at 350 ^{0}C to anneal for 5 minutes. This deposition annealing cycle was repeated 14 times to produce the necessary film thickness. Finally, the substrate was sintered in a tube furnace (MTF 12/38/400, Carbolite) at 550 ^{0}C for 4 hours to produce the final titanium-doped hematite (Ti-Fe_2O_3) films. Electrical connection was made by applying copper tape to the portion of the FTO that was left free of hematite.

Surface characterization

X-ray photoelectron spectroscopy (XPS) measurements were performed on a Kratos Axis ULTRA using focused monochromatized Al Kα (hυ= 1486.61 eV, 15 kV, 225 W, base pressure ≈ 5×10^{-10} Torr) radiation. The binding energy scale was calibrated with hydrocarbon contamination using the C 1s peak at 285 eV. Survey spectra were collected at a constant pass energy of 160 eV from a 0.37 mm² area of the sample. High-resolution spectra of the C 1s, Ti 2p, O 1s and Fe 2p core levels were collected at a pass energy of 20 eV with the same spot size.

Powder XRD measurements were performed on a Rigaku Miniflex. Ti-Fe_2O_3 films on FTO substrates were pressed into ring holders with polyacrylonitrile particles acting as a filler to ensure a tight fit. The source radiation was Cu Kα (40 kV, 15 mA) and was directed through a custom-made1.25 mm-wide divergence slit with a vertical angle of 0.625°. Powder diffractograms were collected while spinning samples at 60 Hz across the range 10°< 2θ <100° using 0.02° steps that lasted for 3 seconds each. Grazing incidence (GI-XRD) diffractograms were acquired on a PANalytical (Philips) X'pert MRD system with a grazing angle of 1.0°. Ti-Fe_2O_3 films on FTO were attached to a glass substrate on the sample holder. The source radiation (Cu Kα, point focus, 45 kV, 40 mA) was passed through a 1.0 x 5.0 mm cross-slit collimator, and the diffracted radiation was detected after passing through a secondary parallel plate collimator and being filtered with a graphite monochromator. A Ni filter was used to filter the incident beam for wide 2-theta scans at 0.05° steps, 0.5 seconds per step; detailed scans at 0.02° steps, 4 seconds per step used unfiltered radiation to increase the signal from the Ti-Fe_2O_3 thin film.

Electrochemical measurements

All electrochemical measurements were performed on either a CHI760 potentiostat or a CHI920D SECM (CHInstruments). Hematite photoanodes were mounted in a custom made SECM cell which leaves a 0.35 cm² area of the hematite substrate electrode exposed to electrolyte. For all experiments, an agar bridged 3 M KCl Ag/AgCl electrode was used as the reference electrode, and potentials reported here are quoted with respect to this reference unless otherwise noted. A 1 mm diameter Pt wire was used as the counter. SECM experiments used a carbon, gold, or platinum disk electrode sealed in a glass capillary (Sutter, Inc.) as the primary working electrode and the hematite substrate as the secondary working electrode. The disk electrodes were fabricated from Au or Pt wires or carbon fibers by traditional methods.[27] Tip electrodes were positioned above the substrate using atmospheric oxygen or the ferri/ferrocyanide ($[Fe(CN)_6]^{3-/4-}$) couple to perform negative feedback approach curves that were fit to established theory.[28] SI-SECM experiments utilized a carbon disk (a = 4 μm) biased to 0 V to perform diffusion limited reduction of potassium ferricyanide (0.2 mM) in a 100 mM borate buffer adjusted to a pH of 9.3 by the addition of NaOH. Hydrogen peroxide (H_2O_2) collection experiments were performed in 100 mM borate buffer (pH 9.3) with a 12.5 μm radius (a) Pt tip biased to +0.4 V to perform diffusion limited oxidation of H_2O_2.

The hematite substrate was illuminated by a 300 W Xe lamp (6258 Oriel) with nearly constant irradiance of 40 mW m^{-2} nm^{-1} in the 300 nm to 800 nm range. Illumination was delivered from the backside of the substrate to prevent light absorption by the electrolyte and ensure uniform illumination of the substrate. Light was directed from the lamp by an optical fiber cable and collimated by a 25mm convex lens as it exited the cable, at which point it had an illumination intensity of 122 mW/cm². It was then reflected off a 45° mirror (ThorLabs CM1F01) into a 10x objective lens which focused the light through the FTO coated glass and onto the hematite substrate. For measurements using white light, the output from the lamp was unfiltered, but for measurements using visible light, lamp output was filtered using a long pass (T<0.1% for λ<405 nm) filter. An Oriel Cornerstone 130 monochromator (Newport) was used to monochromate lamp output for the photoaction spectra and incident photoconversion efficiency (IPCE) measurements.

Numerical Simulations

Finite element simulations were performed using COMSOL v4.4 (COMSOL, Inc.). The framework for the surface interrogation simulations has been described in

detail elsewhere.[23] This framework was modified to simulate two species in the Surface Reactions Module (SRM) with separate individual parameters for the k_{si} and coverage of each. Oxygen collection transients were simulated using the Transport of Diluted Species Module (TDSM). Hydrogen peroxide collection experiments were simulated using both the SRM and the TDSM. Both of these simulations are described in more detail in the supporting information.

RESULTS AND DISCUSSION

Surface characterization

X-ray photoelectron spectroscopy (XPS) measurements were used to confirm the chemical identity of the titanium-doped hematite (Ti-Fe_2O_3) films, the survey spectrum of which can be seen in Fig. S3. High resolution spectra of the Fe 2p region of the spectrum in Fig. 2A shows the Fe $2p_{3/2}$ peak at 711.1 eV and the Fe $2p_{1/2}$ peak at 724.6 eV. Additionally, the satellite peak at 719.3 eV is indicative of the Fe^{3+}, while the absence of a second satellite peak at 717.2 eV shows evidence for the presence of Fe^{2+} in these samples, at least within the detection limits of these XPS experiments. The high resolution Ti 2p XPS spectrum shows a Ti $2p_{3/2}$ peak at 458.4 eV and the Ti $2p_{1/2}$ peak at 464.2 eV. The Fe 2p peak energies are within 0.1 eV of the chemical shifts reported by Wang, et. al. for Ti-Fe_2O_3 on FTO, while the observed Ti 2p peak energies are within 0.2 eV the previously reported positions.[26] Analysis with CasaXPS indicates a Ti doping level of 17% (Table S1). These results indicate that we successfully prepared Ti-doped hematite photoanodes with similar surface properties to previously reported materials.

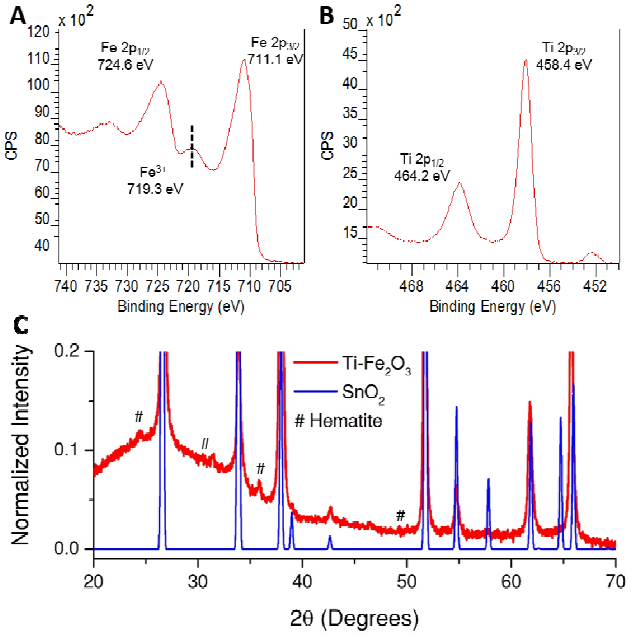

Figure 2: X-ray photoelectron spectroscopy and diffractograms for the prepared hematite electrodes. High resolution taken in (A) Fe 2p and (B) Ti 2p XPS spectra of a Ti-Fe_2O_3 film. The measured chemical shifts for the Fe 2p peaks are within 0.1 eV of what those reported by Wang, et. al, while for the Ti 2p, they are within 0.2 eV. (C) Shows a powder XRD pattern taken of a Ti-Fe_2O_3 film on an FTO substrate in comparison to a SnO_2 standard.

Powder XRD measurements of the hematite photoanodes give an XRD pattern that is dominated by a SnO_2 signal, as shown in Figure 2C. This can be attributed to the FTO film having a thickness much greater than that of the hematite film. By comparing the Ti-Fe_2O_3 film to the SnO_2 standard, the hematite peaks can be identified from the low intensity peaks which are unaccounted for by the SnO_2 signal. Among the low intensity signals there are peaks at 2θ = 24.5°, 30.5°, 35.8°, and 49.3° that were previously identified as belonging to α-Fe_2O_3 that only emerge following sintering of the Ti-Fe_2O_3 films.[26] To ensure higher signals from the Ti-Fe_2O_3 thin film, GI-XRD measurements were taken. Once again, the SnO_2 peaks dominate, but three hematite peaks are apparent at 2θ = 33.2°, 35.8°, 54.0° (Figures S4-S6). The (104) and (116) peaks of α-Fe_2O_3 are partially obscured by SnO_2 peaks and appear as shoulders, but their appearance along with the (110) peak nonetheless verifies the hematite phase over another iron oxide. Combined with the XPS measurements, these results confirm that we have successfully produced Ti-doped hematite films with similar crystalline structures to those previously described by Wang, et al.[26]

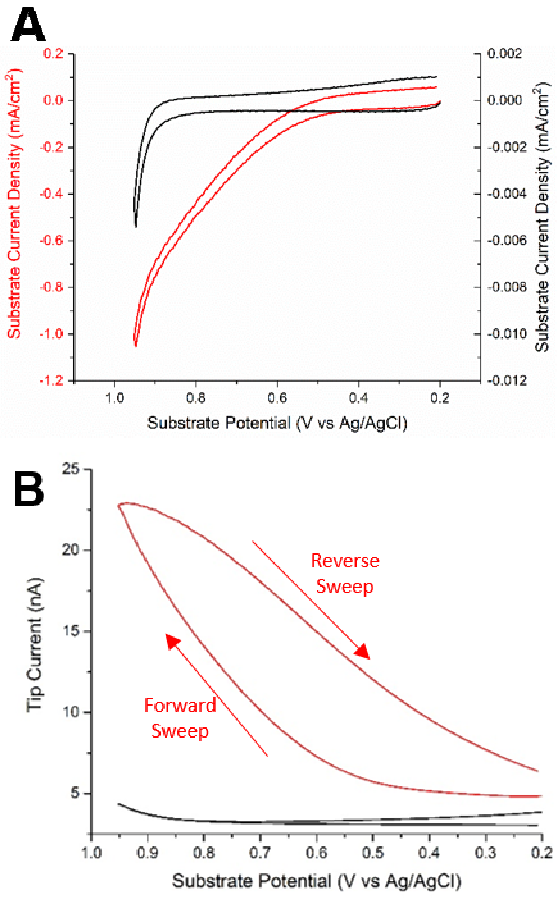

Figure 3: (A) Cyclic voltammograms of a Ti-Fe_2O_3 electrode in the dark (black curve) and under broadband illumination (red curve) recorded in 0.1 M NaOH. (B) Current recorded by a 12.5 μm radius Pt electrode positioned close to the surface and biased at -0.4 V to reduce oxygen during the substrate CVs shown in A.

Bulk photoelectrochemistry

The Ti-Fe_2O_3 exhibited photocatalytic oxygen evolution activity under both UV and visible illumination. As shown in Figure 3A, cyclic voltammograms (CVs) of the Ti-Fe_2O_3 electrodes recorded in 0.1 M NaOH without illumination produced little Faradaic current until +0.85 V. In contrast, CVs under broadband illumination shows an onset potential for water oxidation around +0.3 V. As the spot size of our incident light has a radius of approximately 0.05 cm, the current densities we measured are comparable previous reports of samples fabricated using this protocol.[26] Illumination under only visible light ($\lambda > 405$ nm) shows similar behavior, but with a lower current that correlates well to the integrated IPCE for different illumination conditions, as shown in the supporting information. Figure 3B shows the oxygen collection current (i.e. from reduction of photogenerated O_2 at the tip) measured at a Au disk electrode (a=12.5 μm) positioned 0.9 tip radii (L) from the Ti-Fe_2O_3 surface, as a function of the substrate potential during the CVs in Figure 3A. In the dark, no oxygen is detected until the substrate reaches +0.85 V, consistent with our bulk voltammetry. When the substrate is illuminated, we clearly see during the forward sweep that the oxygen reduction current closely follows the substrate current. In the backward sweep, tip current decreases less rapidly than the substrate current because of the buildup of O_2 generated in the forward sweep. Numerical simulations of this system show that given our estimated current densities, at least 90% of the substrate current would be from the oxidation of water to oxygen. Together, these data show that these Ti-Fe_2O_3 electrodes can perform photoelectrochemical water oxidation using either broadband or visible light.

A first approach to detecting adsorbed intermediates during water oxidation on Ti-Fe_2O_3 is possible by the potential step-sweep function reported recently by Klahr, et al.[7] In this technique, RSSs are generated by biasing the hematite substrate under illumination. Once steady state water oxidation is achieved, illumination is removed and the substrate is quickly scanned negatively to reduce surface species generated in the previous step. As shown in Figure 4A, the cathodic scan produces a reduction peak centered around +0.3 V for all activating potentials. A second reduction peak around +1.0 V appears at activating potentials above +0.9 V. Plotting the observed peak currents versus the scan rate, as shown in Figure 4B, produces a linear relationship, suggesting that both reductions are surface processes. Both peaks increased in size when a more positive bias was used during the potential step. The total charge collected from the sweep reached a limiting value of 5.5 μC under high biases and long illumination times, corresponding to a coverage of 6.4 C/m², based on our illuminated area. However, we were unable to decouple the contributions from each peak and this approach likely underestimates the limiting coverage due to the inability to bias the electrode beyond potentials where hydrogen evolution begins. Together, these behaviors suggest that the two peaks may be reductions of photogenerated intermediates formed on the hematite surface during water oxidation.[7] The RSS reduced at +1.0 V likely has a higher activation energy than the RSS reduced at +0.3 V and therefore attains a high coverage only at more activating bias, while the second species is formed more easily. These measurements provide some evidence that photoassisted water oxidation on hematite may include multiple intermediates, but it is necessary to unambiguously distinguish these populations of RSS to understand their implications for the performance of hematite photoanodes.

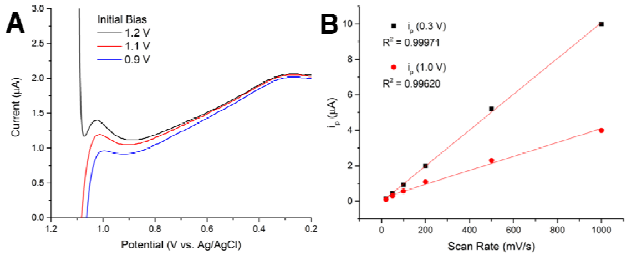

Figure 4: (A) Cathodic scans after activating the hematite substrate at the indicated bias under white light illumination. Peaks appear as surface species are being reduced. (B) Peak current exhibits a linear dependence on scan rate, confirming this is a surface process.

SI-SECM of reactive intermediates

Having characterized the photocatalytic activity of our Ti-Fe_2O_3 we turn to SI-SECM to correlate these results with the reactivity and coverage of RSS. A representative semi-logarithmic plot of the interrogation current recorded after performing the oxygen evolution reaction while biasing the substrate at 0.9 V is shown alongside simulated data in Figure 5A. The initial rise of the interrogation current appears due to the establishment of the positive feedback loop depicted in Figure 1A. The magnitude of this feedback quickly begins to decay as reactive adsorbates closest to the tip are consumed, causing the interrogation current to decrease as the titration continues. At longer time scales (ca. 1 s) a shoulder appears in the data, which is incompatible with the expected interrogation current for a titration of one species with a single characteristic k_{si}. As shown in Figure 5A, simulated interrogations of a single species have one characteristic peak, after which they monotonically decrease to zero. A shoulder such as this only appears in simulated interrogations when a second reactive adsorbed species with a k_{si} differing by at least a factor of 10 is present on the surface. It is important to note that this additional species may in fact have the same chemical identity as the first, but may be reacting at a different rate due to interaction with the substrate.[24] Adding this second species to our simulations allowed us to obtain reasonable agreement between our experimental and simulated results in all cases. A better fit might have been obtained by increasing the number of simulated species, but we believe that the experimentally observed peaks are not resolved enough to justify increasing the number of species beyond two. However, this two-species model allows us to quantify both the coverage and reactivity of two reactive intermediates from a single interrogation.

Table 1: Surface coverage and kinetics of Species 1 and Species 2 from finite element simulations

Substrate Bias (V vs. Ag/AgCl)		0.5	0.7	0.8	0.9	1.0	1.1	k_{si} (m^3/mol s)
Γ_1 (C/m2)	UV/Vis	0.01	0.035	0.07	0.14	0.38	0.85	316±15
	Vis Only	0.02	0.04	0.04	0.02	0.03		316±15
Γ_2 (C/m2)	UV/Vis	0.1	0.6	1.5	3.2	4.9	6.4	2±1
	Vis Only	0.2	0.3	0.4	0.4	0.5		2±1

Interrogation currents and simulated fits are shown in Figure 5B for a series of measurements using increasingly positive substrate biases during the photocatalytic step. It is immediately apparent that the observed feedback increases as the substrate is further activated to perform water oxidation, but also that the interrogation current peaks and shoulders occur at a similar timescale at all potentials. All of these fit well to our two-species model, from which we were able to extract the surface coverages (Q_1 and Q_2) and reaction constants (k_{si1} and k_{si2}) for the fast reacting (Species 1) and slow reacting (Species 2) species shown in Table 1. The data show that although the coverage of both surface species increases with increasing substrate activation, their reactivity remains constant within this potential range. We believe that this trend suggests that the mechanism of water oxidation does not change between these potentials, and that changes in photocurrent are primarily a function of the surface coverage of intermediates. This is further supported by the data in Figure 6, which plots both the total surface coverage and substrate photocurrent measured using broadband or visible light illumination against substrate bias potential. The differences in coverage between visible and white light illumination correlate well to the differences in integrated IPCE for the ranges of light in either experiment (see Supporting Information). All of these relationships strongly suggest that the species we are titrating are intermediates of the water oxidation reaction.

Our detection of RSS with differing reactivities can be the result of having two distinct chemical species adsorbed to the surface that react with our mediator at different rates. However, this observation could also be due to substrate-adsorbate interactions modulating the kinetics of a single adsorbed species and changing the observed kinetics, thus we require complementary information to differentiate these possibilities. The most well characterized metal oxide photocatalyst, TiO_2, is well known to produce hydroxyl radicals (•OH) that are critical to many photocatalytic functions of TiO_2.[29-31] The identity of oxidizing species formed on hematite during photoactivity are less well characterized.[2] As the reactivity of Species 1 is reasonably close to what has been observed before for RSS on TiO_2[20] and $SrTiO_3$,[23] we investigated the possibility that $•OH_{(ads)}$ was one of the species we detected.

The rate at which intermediates decay on a reactive surface can be measured using SI-SECM by introducing a delay between the substrate activation and tip titration steps of the experiment. This allows us to measure the coverage of intermediates as a function of delay time. Previous SI-SECM studies have used this to study the decay of photogenerated surface species on TiO_2[20] and W/Mo-$BiVO_4$.[21] Decay kinetics observed in both of these cases fit well to second order reaction kinetics, and as such were attributed to the dimerization of •OH to form H_2O_2. Shown in Figure 7A are delayed interrogations performed on a Ti-Fe_2O_3 sample after photocatalytic steps with a substrate biases of 0.9 to 1.1 V. The surface coverages of both species are extracted from this

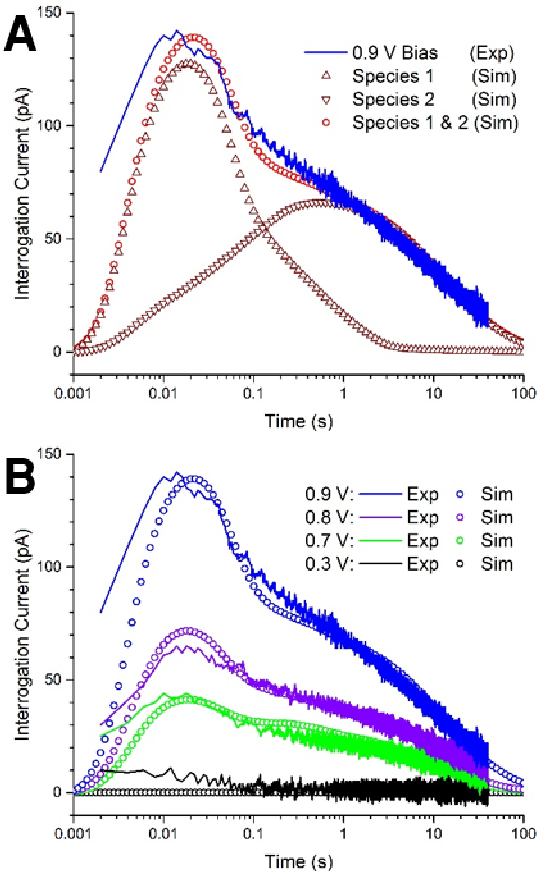

Figure 5: (A) Experimental interrogation current collected after a bias of 0.9 V (blue line). Best fits modeled with a single fast reacting species (up triangles), with a single slow reacting species (down triangle), and a linear combination of the two (red circles), are overlaid. (B) Best fits to experimental data using the two species model for a range of activating potentials. Satisfactory fitting of experimental data is achieved over several orders of magnitude in time. Interrogations were performed with a 4 µm carbon disk electrode in an aqueous solution of 50 µM ferricyanide in 100 mM borate buffer (pH=9.3) under broadband illumination.

data and plotted as a function of delay time in accordance second order

integrated rate law in Figure 7B. The decreasing coverages fit well to second order decay kinetics for all of these potentials, but lower potentials are not included because the interrogation signals were too low to reliably extract coverages at long delay times. Species 1 and 2 fit well to a second order decay constants (k_d) of $1.2\times10^5 \pm 0.2\times10^5$ and $6.3\times10^3 \pm 0.9\times10^3$ $m^2/(mol\cdot s)$, respectively. The decay rate for species 2 is close to that reported by the Bard group previously for decay of reactive surface species on TiO_2[20]and $BiVO_4$[21] microelectrodes. Decay kinetics observed on W/Mo-$BiVO_4$ and TiO_2 were attributed to the dimerization of •OH to form H_2O_2. Therefore, we searched for further evidence of this reaction by probing for H_2O_2 generation near the surface of our Ti-Fe_2O_3 film.

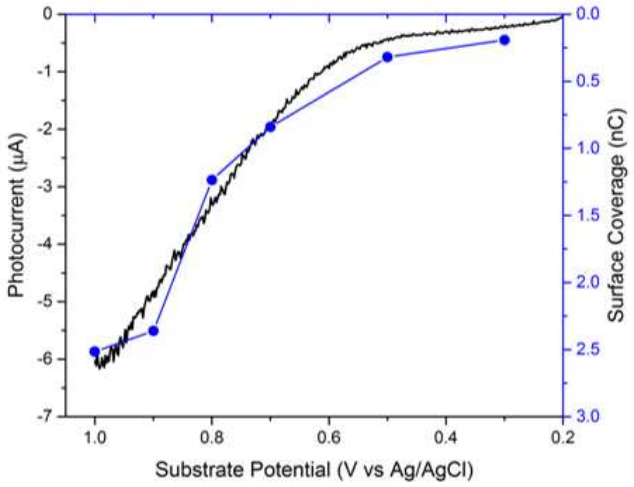

Figure 6: Total charge collected by SI-SECM (blue circles) overlaid on a I(V) curve of Hematite (black line).

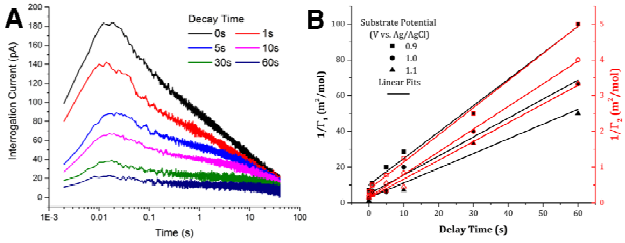

Figure 7: (A) Surface interrogations recorded after a delay that followed substrate activation at 0.9 V vs Ag/AgCl for 40 s show a decreasing interrogation current as the delay increases. (B) Coverages of species 1 and 2 as a function of delay time fit to second order kinetics. The plotted fits give the disproportionation kinetics as $k_{d1}=1.2\times10^5 \pm 0.2\times10^5$ and $k_{d2}=6.3\times10^3 \pm 0.9\times10^3$ $m^2/(mol\cdot s)$.

Transient detection of discharge products from adlayer

We now turn to a transient application of SECM in the substrate generation / tip collection mode (SG/TC) for quantitatively correlating the formation of H_2O_2 to the measured surface intermediates. The detection of hydrogen peroxide has previously been used as an indirect verification for the presence of $•OH_{(ads)}$ in other photocatalytic systems.[32] Many of these studies rely on colorimetric methods involving the addition of a colorimetric[33] or fluorescent[34] indicator to the solution. Many indicators can be oxidized by species other than H_2O_2, or reduced by conduction band electrons when illumination is removed.[31] In contrast to these methods, SG/TC SECM experiments are ideal for the quantification of H_2O_2 formed after photocatalysis because of its selectivity towards solution species, excellent detection limits, and temporal resolution.[35] As shown in Figure 8A, any $•OH_{(ads)}$ from the water oxidation reaction that reacts to form H_2O_2, can be detected when it is oxidized at the probe electrode. The resulting current magnitude can be used to quantify the amount of H_2O_2 generated at the substrate.

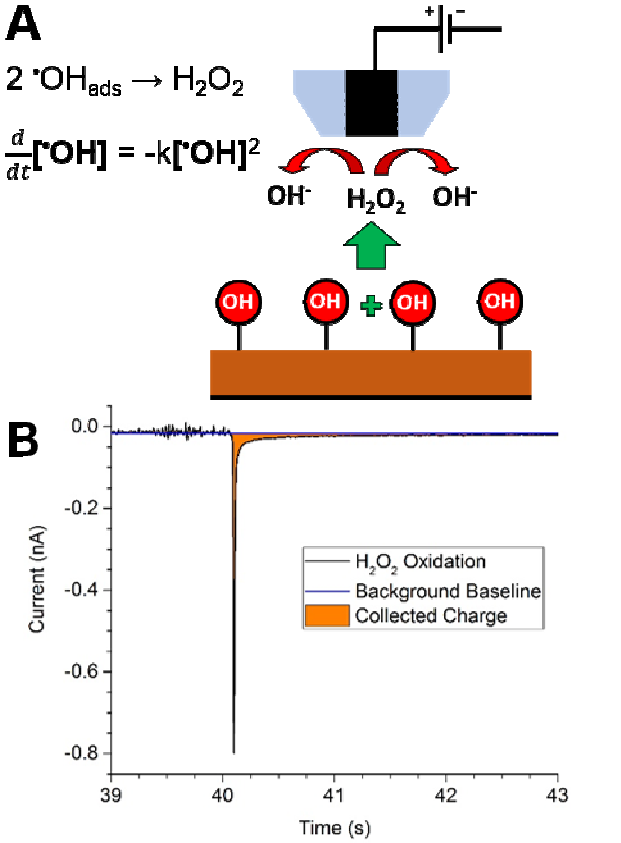

Figure 8: (A) Schematic of the tip collection step of transient hydrogen peroxide collection experiments. (B)Tip current as a function of time during a transient substrate generation tip collection experiment. In this setup, a 12.5 μm tip electrode is positioned 10 μm from the surface and biased at 0.40 V for the duration of the experiment. The substrate is activated to perform steady state water oxidation for the first 40 seconds. Substrate illumination and bias are removed after 40 seconds while continuing to record tip current.

A typical result of the transient SG/TC experiment is shown in Figure 8B. For the first 40 seconds, hematite is activated with bias and illumination to perform steady state water oxidation. The tip registers only a small background current during this time. After 40 seconds, illumination is removed to halt substrate activity. The tip response is an initial spike in oxidative current which quickly decays to the same background level as before. The fact that background current levels are identical during and

after substrate activity indicates this background current is not a result of products from photocatalytic reactions at the hematite surface. This implies H_2O_2 is not produced as part of a parasitic side reaction during electrode operation. The spike in current is presumably collection of H_2O_2 produced by the decay of unconsumed $•OH_{(ads)}$. Integration of this peak using the background current as a baseline provides the charge collected by the tip. At a +0.9 V substrate bias, 82 pC of hydrogen peroxide were collected. Given a probe electrode area of 491 μm^2, if a collection efficiency of 100% is assumed, we calculate a minimum needed surface coverage of 0.17 C/m^2 of $•OH_{(ads)}$. This value is very close to the value of Γ_1 (0.14 C/m^2) measured *via* SI-SECM for this bias potential, but far lower than what is predicted for Species 2 (3.2 C/m^2).

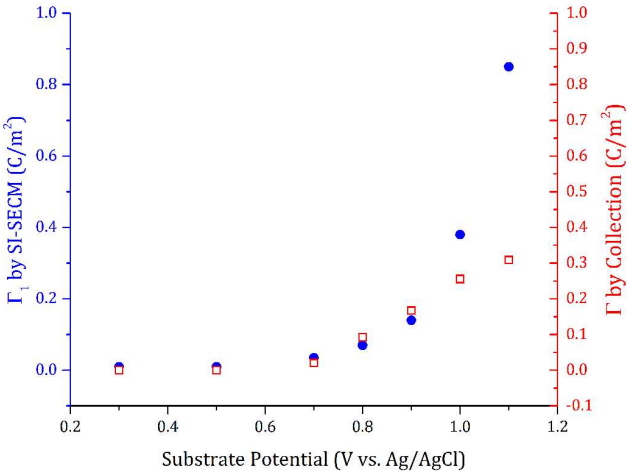

Figure 9: Comparison of the coverage of species 1 as measured by SI-SECM to the charge collected in SG/TC experiments.

The total charge of H_2O_2 measured at other bias potentials by transient SG/TC are shown in Figure 9 alongside the coverage of Species 1 from Table 1. This graph demonstrates an excellent correlation between surface coverages measurements made through SI-SECM that only deviates at high potentials, where the electrocatalytic activity of the substrate significantly contributes to observed current. Despite these deviations, the correlation between our transient SG/TC experiments and our SI-SECM measurements provides strong evidence for the presence of $•OH_{(ads)}$ that undergoes decomposition to H_2O_2 on these hematite photoanodes.

CONCLUSIONS

SI-SECM was used to quantify the coverage and reactivity of RSS at operating hematite photoanodes. Fitting of the current response indicated the coexistence of 2 distinct populations of surface species reacting with individual rate constants. These interrogation rate constants did not change as a function of substrate activation, showing the identity of RSS does not change with increasing bias. The decay of these species was found to follow a second order process. Hydrogen peroxide was identified as a likely product of this decay using a transient SG/TC mode of SECM. The charge collected by SG/TC SECM during open-circuit discharge experiments correlates well to that obtained for species 1 obtained by surface-sensitive measurements using SI-SECM. This provides strong evidence for the existence of the $•OH_{(ads)}$ intermediate on hematite electrodes and clearly shows a mechanism for the generation of unwanted products in photoelectrochemical cells when switching between active and inactive states.

Confirmation of the of chemical identity of the slow reacting species as $•OH_{(ads)}$, and the identification of the second population of surface species remain open challenges. As we demonstrated here, SI-SECM a powerful method for direct, quantitative detection of multiple surface intermediates simultaneously. While other techniques have shown evidence of multiple RSS at the surface,[7] these experiments directly showed that both of these species can participate in interfacial reactivity. SI-SECM quantifies these RSS *in situ*, which is vital to understanding the energetics of these water oxidation intermediates. Our group recently demonstrated the use of SI-SECM coupled to Raman spectroscopy, which adds chemical information to complement the precise quantification possible by SI-SECM.[36] Although the Raman signal from the reactive surface species is below the sensitivity of our instrument, future work using techniques to enhance the Raman signal may enable *operando* identification and quantification of these surface species. Combined with other modes of SECM, SI-SECM allows deep mechanistic insight into the surface chemistry of operating catalytic interfaces. Our development of the simulations needed to identify multiple surface intermediates by their reactivity will make SI-SECM a useful tool for creating experimentally-supported microkinetic models of the complex environments involved in heterogeneous catalysis.

ASSOCIATED CONTENT

Supporting Information

The Supporting Information is available free of charge on the ACS Publications website.

Finite element model details and parameters; XPS survey spectrum; XRD of undoped samples; IPCE measurement; LSVs comparing illumination conditions; additional SI-SECM measurements; UME characterization; and H_2O_2 collection calibration (PDF)

AUTHOR INFORMATION

Corresponding Author

* E-mail: joaquinr@illinois.edu.

Present Addresses

† Division of Chemistry and Chemical Engineering, California Institute of Technology, Pasadena, CA 91125

Author Contributions

‡These authors contributed equally.

ACKNOWLEDGMENT

Materials characterization was carried out in part in the Frederick Seitz Materials Research Laboratory Central Re-

search Facilities at the University of Illinois at Urbana-Champaign. JRL acknowledges support of startup funds from the University of Illinois as well as from the SACP Starter Grant which allowed the construction of the instrument used in this study.

REFERENCES

(1) Sivula, K.; Le Formal, F.; Gratzel, M. *ChemSusChem* **2011**, *4*, 432-449.
(2) Katz, M. J.; Riha, S. C.; Jeong, N. C.; Martinson, A. B. F.; Farha, O. K.; Hupp, J. T. *Coord. Chem. Rev.* **2012**, *256*, 2521-2529.
(3) Iandolo, B.; Wickman, B.; Zoric, I.; Hellman, A. *J. Mater. Chem. A* **2015**, *3*, 16896-16912.
(4) Young, K. M. H.; Klahr, B. M.; Zandi, O.; Hamann, T. W. *Catal. Sci. Technol.* **2013**, *3*, 1660-1671.
(5) Wijayantha, K. G. U.; Saremi-Yarahmadi, S.; Peter, L. M. *PCCP* **2011**, *13*, 5264-5270.
(6) Klahr, B.; Gimenez, S.; Fabregat-Santiago, F.; Hamann, T.; Bisquert, J. *J. Am. Chem. Soc.* **2012**, *134*, 4294-4302.
(7) Klahr, B.; Gimenez, S.; Fabregat-Santiago, F.; Bisquert, J.; Hamann, T. W. *Energy Environ. Sci.* **2012**, *5*, 7626-7636.
(8) Peter, L. M.; Wijayantha, K. G. U.; Tahir, A. A. *Faraday Discuss.* **2012**, *155*, 309-322.
(9) Klotz, D.; Ellis, D. S.; Dotan, H.; Rothschild, A. *Phys. Chem. Chem. Phys.* **2016**, *18*, 23438-23457.
(10) Thorne, J. E.; Jang, J. W.; Liu, E. Y.; Wang, D. W. *Chem. Sci.* **2016**, *7*, 3347-3354.
(11) Barroso, M.; Mesa, C. A.; Pendlebury, S. R.; Cowan, A. J.; Hisatomi, T.; Sivula, K.; Gratzel, M.; Klug, D. R.; Durrant, J. R. *Proc. Natl. Acad. Sci. U.S.A.* **2012**, *109*, 15640-15645.
(12) Huang, Z. Q.; Lin, Y. J.; Xiang, X.; Rodriguez-Cordoba, W.; McDonald, K. J.; Hagen, K. S.; Choi, K. S.; Brunschwig, B. S.; Musaev, D. G.; Hill, C. L.; Wang, D. W.; Lian, T. Q. *Ener. Environ. Sci.* **2012**, *5*, 8923-8926.
(13) Pendlebury, S. R.; Cowan, A. J.; Barroso, M.; Sivula, K.; Ye, J. H.; Gratzel, M.; Klug, D. R.; Tang, J. W.; Durrant, J. R. *Ener. Environ. Sci.* **2012**, *5*, 6304-6312.
(14) Zandi, O.; Hamann, T. W. *Nat. Chem.* **2016**, *8*, 778-783.
(15) Fernandez, J. L.; Bard, A. J. *Anal. Chem.* **2003**, *75*, 2967-2974.
(16) Lee, J. W.; Ye, H. C.; Pan, S. L.; Bard, A. J. *Anal. Chem.* **2008**, *80*, 7445-7450.
(17) Horrocks, B. R.; Mirkin, M. V.; Bard, A. J. *J. Phys. Chem.* **1994**, *98*, 9106-9114.
(18) Haram, S. K.; Bard, A. J. *J. Phys. Chem. B* **2001**, *105*, 8192-8195.
(19) Rodríguez-López, J.; Alpuche-Avilés, M. A.; Bard, A. J. *J. Am. Chem. Soc.* **2008**, *130*, 16985-16995.
(20) Zigah, D.; Rodríguez-López, J.; Bard, A. J. *Phys. Chem. Chem. Phys.* **2012**, *14*, 12764-12772.
(21) Park, H. S.; Leonard, K. C.; Bard, A. J. *J. Phys. Chem. C* **2013**, *117*, 12093-12102.
(22) Arroyo-Currás, N.; Bard, A. J. *J. Phys. Chem. C* **2015**, *119*, 8147-8154.
(23) Simpson, B. H.; Rodríguez-López, J. *Electrochim. Acta* **2015**, *179*, 74-83.
(24) Simpson, B. H.; Rodríguez-López, J. *J. Am. Chem. Soc.* **2015**, *137*, 14865-14868.
(25) Rodríguez-López, J.; Zoski, C. G.; Bard, A. J. In *Scanning Electrochemical Microscopy, Second Edition*; CRC Press, 2012, pp 525-568.
(26) Wang, G. M.; Ling, Y. C.; Wheeler, D. A.; George, K. E. N.; Horsley, K.; Heske, C.; Zhang, J. Z.; Li, Y. *Nano Lett.* **2011**, *11*, 3503-3509.
(27) Bard, A. J.; Faulkner, L. R. *Electrochemical methods : fundamentals and applications*, 2nd ed.; Wiley: New York, 2001, p xxi, 833 p.
(28) Lefrou, C.; Cornut, R. *ChemPhysChem* **2010**, *11*, 547-556.
(29) Nosaka, Y.; Kishimoto, M.; Nishino, J. *J. Phys. Chem. B* **1998**, *102*, 10279-10283.
(30) Nakabayashi, Y.; Nosaka, Y. *J. Phys. Chem. C* **2013**, *117*, 23832-23839.
(31) Zhang, J.; Nosaka, Y. *J. Phys. Chem. C* **2014**, *118*, 10824-10832.
(32) Diesen, V.; Jonsson, M. *J. Phys. Chem. C* **2014**, 5.
(33) Hirakawa, T.; Nosaka, Y. *Langmuir* **2002**, *18*, 3247-3254.
(34) Naito, K.; Tachikawa, T.; Fujitsuka, M.; Majima, T. *J. Phys. Chem. B* **2005**, *109*, 23138-23140.
(35) Mezour, M. A.; Cornut, R.; Hussien, E. M.; Morin, M.; Mauzeroll, J. *Langmuir* **2010**, *26*, 13000-13006.
(36) Gossage, Z. T.; Schorr, N. B.; Hernandez-Burgos, K.; Hui, J.; Simpson, B. H.; Montoto, E. C.; Rodriguez-Lopez, J. *Langmuir* **2017**, *33*, 9455-9463.

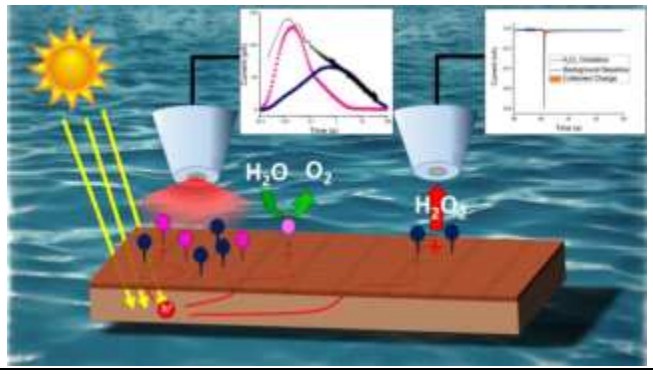
H_2O O_2
H_2O_2